Analytical Modeling of Electrical Characteristics of Low Bandgap Graphene Nanoribbon FET

Md. Shofiqul Islam, Tanvir Muntasir, Shuvomoy Das Gupta

Abstract- In this paper analytical modeling for the electrical characteristics of low bandgap graphene nanoribbon field effect transistor (GNR-FET) has been presented. This analytical modeling is based on the two-dimensional Poisson's equation in the weak nonlocality approximation. At first, analytical formula for spatial distribution of electric potential along the channel of low bandgap GNR-FET has been derived. Then using the channel potential, an expression of drain current of low bandgap GNR-FET is developed. The potential distribution and current are expressed in terms of device parameters and applied voltages. Spatial potential has been investigated with different levels of gate voltage, gate length and drain voltage. Similarly, the current has been investigated with different applied voltages. It shows that drain current is controlled by applied voltages hence the device might be applicable in digital and analog circuits. This work of analytical modeling would be helpful for analyzing the device and optimizing the parameters to improve its performance.

Index Terms— analytical modeling, graphene nanoribbon, GNR-FET, spatial potential, low bandgap.

I. INTRODUCTION

Silicon has been unparallel candidate in semiconductor industry since long years. However, silicon based technology has reached to its upper physical limits of design complexity, processing power, energy consumption, density and heat dissipation [1]. While Si-based technology is approaching its fundamental limits, the researchers are working to find out new candidate material to replace Si to overcome the limitations [2]. Recently, grapheme is attracting the attention of the researchers because of high mobility for ballistic transport, high carrier velocity for fast switching, monolayer thin body for optimum electrostatic scaling, excellent thermal conductivity [3]. Therefore, graphene might be an alternate choice instead of Si. Graphene is one atom thick planer sheets of sp^2 bonded carbon atoms, which are densely packed in a honeycomb crystal lattice [2]. Graphene sheet has zero bandgap but if graphene is fabricated as an array of strips, then it provides sufficient band gap for switching [3]; these strips are called graphene nanoribbons (GNR). Patterned graphene, that consists of an array of graphene strips, provides an opportunity to engineer the band structure [4]. New devices based on electrically induced p-n junctions, utilizing graphene nanoribbons as the channel material has been reported [5]. A graphene-based field-effect-transistor with an n+-Si substrate serving as a back gate and a metal serving as a top gate, has been fabricated and characterized [6]. The operation of the GNR-FET is accompanied by formation of the lateral n-p-n junction in the channel and the energy barrier [4]. In the channel, the p-type region is formed under the top gate applying sufficiently strong negative bias on the top gate. In this case, the GNR-FET channel is partitioned into three sections: the source n-section, the p-section under the top gate and the drain n-section, thus a lateral n-p-n junction is formed in the channel [7]. Literature shows that the current-voltage characteristics of GNR-FET, which is fabricated with high bandgap GNR, have been analyzed by Ryzhii *et al.* [4]. However, to have high bandgap GNR, the strips of graphene should be very narrow since band gap of grapheme nanoribbons is inversely related to the width of the graphene nanoribbons [8]. But fabricating very narrow strips of graphene is challenging because of physical limitations of fabrication process and tools. On the other hand, fabricating GNR with higher width would be less challenging and more feasible. Graphene nanoribbon with higher width has lower band gap, still sufficient for switching operation and has application in digital and analog circuits [3]. Considering the feasibility of fabrication, attention should be given to analyze GNR-FET that utilizes GNR with higher width, i.e. low bandgap GNR-FET. However, there are few reports on analysis of such low bandgap GNR-FET in the literature. In this paper analytical modeling of electrical characteristics of low bandgap GNR-FET has been presented which will enrich the literature on low bandgap GNR-FET.

To derive drain current, potential profile in the channel is required. So, the analytical formula for potential distribution along the channel is developed and analyzed at first and then analytical equation of drain current is developed and investigated. This work would fill the deficit of analyzing low bandgap GNR-FET and serve to improve its performance by optimizing the parameters.

II. DEVICE STRUCTURE

The device structure of GNR-FET considered in this work is shown in Fig.1. The figure shows common source configuration. The device has two gates: top gate and back gate. Graphene nanoribbons are used as channel. An electron channel is formed in the GNR between the ohmic source and drain contacts because of the application of positive voltage at the back gate. Graphene nanoribbons are shown Fig 2.

Revised Version Manuscript Received on September 10, 2015.

Md. Shofiqul Islam, Department of Electrical and Computer Engineering, Faculty of Engineering, King Abdulaziz University, PO Box 80204, Jeddah 21589, Saudi Arabia.

Tanvir Muntasir, Department of Electrical and Computer Engineering, Iowa State University, Ames, Iowa 50011, USA.

Shuvomoy Das Gupta, Department of Electrical and Computer Engineering, University of Toronto, Ontario, Canada.

Published By:
Blue Eyes Intelligence Engineering
& Sciences Publication Pvt. Ltd.

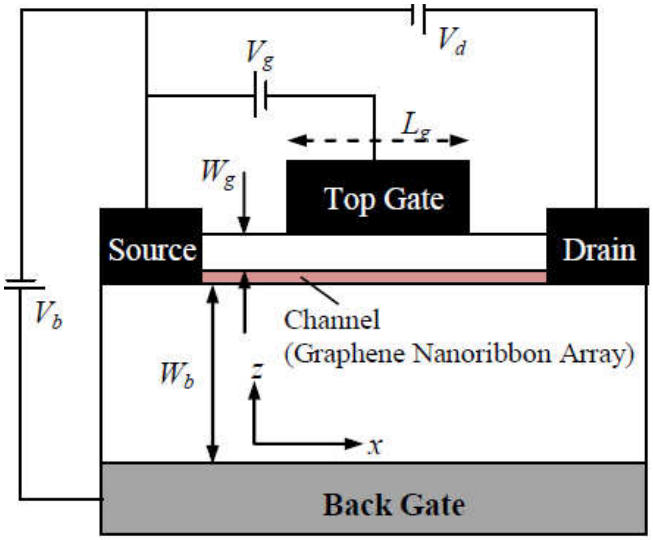

Fig. 1 Schematic view of graphene nanoribbon field effect transistor (GNR-FET) structure. Here, V_g= top gate voltage, V_b= back gate voltage, V_d= drain voltage, W_b= thickness of insulating layer between graphene-nanoribbons and back gate, W_g= thickness of insulating layer between graphene-nanoribbons and top gate, L_g= length of the top gate.

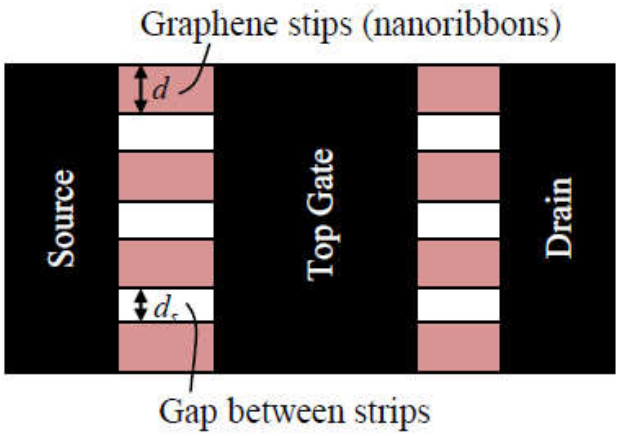

Fig. 2 Top view of GNR-FET showing graphene nanoribbon strips. Here *d* is the width of graphene strip and *ds* is the separation between two adjacent strips.

The positive back gate voltage is sufficiently high to induce the necessary electron density in the source and drain section. The top gate controls the drain current by forming the energy barrier for the electrons propagating between source and drain contacts.

The energy gap is electrically induced by the back gate voltage [4]. The GNR-FET is based on a patterned graphene layer that constitutes a dense array of parallel nanoribbons of width d and the spacing between the nanoribbons is d_s where $d_s << d$, as shown in Fig. 2. The two edges of nanoribbons are connected to conducting pads acting as the transistor source and drain. The back gate is a highly conducting substrate.

III. Potential Distribution

A. Derivation of the Differential Equation Governing the Potential Distribution

The active region of GNR-FET region is under the top gate, which is defined as : $-L_g/2 < x < L_g/2$ and $-W_b < z < W_g$. Here the axis x is directed along the nanoribbons, whereas the axis z is directed perpendicular to the nanoribbons and the gate planes (Fig. 1). Here L_g is the gate length, W_b is the layer thickness between GNR layer and back gate, W_g is the layer thickness between GNR layer and top gate. The main equation governing the spatial distribution of the electric potential (φ) in the active region of the transistor channel is stated as follows [4], [9], [10].

$$\frac{W_b+W_g}{3}\frac{d^2\varphi}{dx^2}-\frac{\varphi-V_b}{W_b}-\frac{\varphi-V_g}{W_g}=\frac{4\pi e}{\varepsilon}\left(\sum\nolimits_- -\sum\nolimits_+\right) \quad (1)$$

With the boundary conditions,

$$\varphi\left(x=-\frac{L_g}{2}\right)=0,\ \varphi\left(x=\frac{L_g}{2}\right)=V_d \quad (2)$$

This equation is a consequence of the two-dimensional Poisson's equation in the weak nonlocality approximation [9],[10]. Here φ corresponds to the electric potential along the channel, e is the charge of electron, ε is dielectric constant (relative permittivity) of the insulating material separating the channel from the gate, $\sum_-$ and $\sum_+$ are electron and hole sheet densities in the channel respectively.

The electron and hole densities in the source and drain regions are related to the Fermi energy, which is reckoned from the middle of the band gap, as follows [4].

$$\sum\nolimits_{\mp}^{s}=\frac{4}{\pi\hbar dv}\exp\left(\pm\frac{E_F^s+e\varphi}{K_BT}\right)\int_{\Delta/2}^{\infty}\frac{E\exp\left(-E/K_BT\right)}{\sqrt{E^2-\Delta^2/4}}dE \quad (3)$$

$$\sum\nolimits_{\mp}^{d}=\frac{4}{\pi\hbar dv}\exp\left(\pm\frac{E_F^d+e(\varphi-V_d)}{K_BT}\right)\int_{\Delta/2}^{\infty}\frac{E\exp\left(-E/K_BT\right)}{\sqrt{E^2-\Delta^2/4}}dE \quad (4)$$

Here, $\hbar$ is reduced Plank's constant, v is the characteristic velocity of charge carrier, band gap $\Delta=2\pi v\hbar/d$, E_F is the Fermi energy in the source region with superscript 's' and in the drain region with superscript 'd', K_B is Boltzmann constant and T is temperature. It is to note that since band gap $\Delta=2\pi v\hbar/d$, Δ (bandgap) is reduced for larger d (nanoribbon width).

The following equations can be derived from (3) and (4).

$$\sum\nolimits_{\mp}^{s}=\left(\frac{2\Delta}{\pi\hbar dv}\right)\exp\left(\pm\frac{E_F^s+e\varphi}{K_BT}\right)K_1\left(\frac{\Delta}{2K_BT}\right) \quad (5)$$

$$\sum\nolimits_{\mp}^{d}=\left(\frac{2\Delta}{\pi\hbar dv}\right)\exp\left(\pm\frac{E_F^d+e(\varphi-V_d)}{K_BT}\right)K_1\left(\frac{\Delta}{2K_BT}\right) \quad (6)$$

Here, $K_1(\Delta/(2K_BT))$ is the modified Bessel function of first order. When bandgap (Δ) is very low, then $\Delta/(2K_BT)$ would be less than unity, i.e. $(\Delta/(2K_BT))<<1$; this condition would be more strongly valid at high temperature when K_BT becomes larger. Under the condition of $(\Delta/(2K_BT))<<1$, the value of $K_1(\Delta/(2K_BT))$can be approximated. According to mathematics, the asymptotic approximation of Bessel function $K_1(\zeta)$ for $\zeta<<1$ is,

$$\lim_{\zeta\to o} k_1(\zeta)=\frac{1}{\zeta} \quad (7)$$

So, for low bandgap nanoribbons, the value of $K_1(\Delta/(2K_BT))$ becomes $(2K_BT)/\Delta$. Then equations (5) and (6) take the following forms.

$$\sum\nolimits_{\mp}^{s}=\left(\frac{4K_BT}{\pi\hbar dv}\right)\exp\left(\pm\frac{E_F^s+e\varphi}{K_BT}\right) \quad (8)$$

$$\sum\nolimits_{\mp}^{d}=\left(\frac{4K_BT}{\pi\hbar dv}\right)\exp\left(\pm\frac{E_F^d+e(\varphi-V_d)}{K_BT}\right) \quad (9)$$

At the source position potential, $\varphi = 0$, therefore, at source $\sum_{-,0}^{s}-\sum_{+,0}^{s}=\varepsilon V_b/4\pi eW_b$; at the drain position potential, $\varphi=V_d$,

Published By:
Blue Eyes Intelligence Engineering
& Sciences Publication Pvt. Ltd.

therefore, at drain $\sum_{-,0}^{d} - \sum_{+,0}^{d} = \varepsilon(V_b - V_d)/4\pi e W_b$ [4]. Here the quantities with the index '0' are the electron and hole densities in the immediate vicinity of the source and drain contacts. Under this consideration the following equations can be derived.

$$\sinh\left(\frac{E_F^s}{K_B T}\right) = \left(\frac{\varepsilon V_b \hbar dv}{32 e W_b}\right)\left(\frac{1}{K_B T}\right) \quad (10)$$

$$\sinh\left(\frac{E_F^d}{K_B T}\right) = \left(\frac{\varepsilon (V_b - V_d) \hbar dv}{32 e W_b}\right)\left(\frac{1}{K_B T}\right) \quad (11)$$

Above two equations give us the value of Fermi energy in the source and drain region as follows.

$$E_F^s = (K_B T)\sinh^{-1}\left[\left(\frac{\varepsilon V_b \hbar dv}{32 e W_b}\right)\left(\frac{1}{K_B T}\right)\right] \quad (12)$$

$$E_F^d = (K_B T)\sinh^{-1}\left[\left(\frac{\varepsilon (V_b - V_d) \hbar dv}{32 e W_b}\right)\left(\frac{1}{K_B T}\right)\right] \quad (13)$$

Using above values of Fermi energy in the source and drain region, the following equations can be found from (8) and (9).

$$\sum_{\mp}^{s} = \left(\frac{4 K_B T}{\pi \hbar dv}\right)\exp\left(\pm\frac{e\varphi}{K_B T}\right)\times \exp\left(\pm\sinh^{-1}\left[\left(\frac{\varepsilon V_b \hbar dv}{32 e W_b}\right)\left(\frac{1}{K_B T}\right)\right]\right) \quad (14)$$

$$\sum_{\mp}^{d} = \left(\frac{4 K_B T}{\pi \hbar dv}\right)\exp\left(\pm\frac{e(\varphi - V_d)}{K_B T}\right)\times \exp\left(\pm\sinh^{-1}\left[\left(\frac{\varepsilon (V_b - V_d) \hbar dv}{32 e W_b}\right)\left(\frac{1}{K_B T}\right)\right]\right) \quad (15)$$

The above equations state the relationship of the electron and hole density with the electric potential. Using these relations in equation (1), we can arrive at the following equations which govern the potential distribution under the top gate in the active region.

$$\frac{d^2\varphi}{dx^2} - \frac{3}{W_b W_g}\varphi = -\frac{3}{W_b + W_g}\left(\frac{V_b}{W_b} + \frac{V_g}{W_g}\right) + \left(\frac{96}{W_b + W_g}\right)\left(\frac{e K_B T}{\varepsilon \hbar dv}\right)\sinh\left(\frac{e\varphi}{K_B T} + \sinh^{-1}\left[\left(\frac{\varepsilon V_b \hbar dv}{32 e W_b}\right)\left(\frac{1}{K_B T}\right)\right]\right) \quad (16)$$

$$\frac{d^2\varphi}{dx^2} - \frac{3}{W_b W_g}\varphi = -\frac{3}{W_b + W_g}\left(\frac{V_b}{W_b} + \frac{V_g}{W_g}\right) + \left(\frac{96}{W_b + W_g}\right)\left(\frac{e K_B T}{\varepsilon \hbar dv}\right)\times \sinh\left(\frac{e(\varphi - V_d)}{K_B T} + \sinh^{-1}\left[\left(\frac{\varepsilon (V_b - V_d) \hbar dv}{32 e W_b}\right)\left(\frac{1}{K_B T}\right)\right]\right) \quad (17)$$

B. Spatial Distribution of Potential along the Channel

Either (16) or (17) may be solved to get the potential (φ) equation as the function of x (i.e. position) to obtain the spatial distribution of potential. We are solving (16) here. For graphene-nanoribbons with lower band gap, the energy barrier for electrons propagating between source and drain contact, gets reduced. In this situation, the value of electric potential (φ) is very low but still drain current is controllable. Using the formula, $\sinh(x+a)=\sinh(a)+(\cosh(a))x$, when x is very small, the last term of (16) can be expanded as below.

$$\sinh\left(\frac{e\varphi}{K_B T} + \sinh^{-1}\left[\left(\frac{\varepsilon V_b \hbar dv}{32 e W_b}\right)\left(\frac{1}{K_B T}\right)\right]\right) = \frac{\varepsilon V_b \hbar dv}{32 e W_b K_B T} + \sqrt{1 + \left(\frac{\varepsilon V_b \hbar dv}{32 e W_b K_B T}\right)^2}\,\frac{e\varphi}{K_B T}$$

Finally, (16) can be presented in the following form,

$$\frac{d^2\varphi}{dx^2} - \frac{3}{W_b W_g}\varphi = -\frac{3}{W_b + W_g}\left(\frac{V_b}{W_b} + \frac{V_g}{W_g}\right) + \left(\frac{96}{W_b + W_g}\right)\left(\frac{e K_B T}{\varepsilon \hbar dv}\right)\left[\frac{\varepsilon V_b \hbar dv}{32 e W_b K_B T} + \sqrt{1 + \left(\frac{\varepsilon V_b \hbar dv}{32 e W_b K_B T}\right)^2}\,\frac{e\varphi}{K_B T}\right] \quad (18)$$

Solving (18) by using the boundary condition stated (2), we get the following equation.

$$\varphi = V_d\,\frac{\sinh\left(A\left(x + \frac{L_g}{2}\right)\right)}{\sinh\left(A L_g\right)} + V_g\,\frac{1}{A^2}\left(-\frac{3}{W_b W_g + W_g^2}\right)\left(\frac{\cosh(Ax)}{\cosh\left(A\frac{L_g}{2}\right)} - 1\right) \quad (19)$$

Here,

$$A = \sqrt{B + C\sqrt{1 + D V_b^2}};\; B = \frac{3}{W_b W_g};\; C = \frac{96 e^2}{dv \varepsilon \hbar (W_b + W_g)};$$

$$D = \frac{\varepsilon^2 \hbar^2 d^2 v^2}{1024 e^2 T^2 K_B^2 W_b^2}$$

We know, corresponding to each potential (φ), the barrier for electron is $-e\varphi$. The minimum potential will correspond to maximum barrier for electrons and maximum barrier will decide the current. Therefore, minimum potential is a factor to be used to determine the current equation. The minimum value of φ exists at $x = 0$. Putting $x = 0$ in (19), we get the following equation of the minimum value of the electric potential (φ_m).

$$\varphi_m = V_d\,\frac{\sinh\left(A L_g/2\right)}{\sinh\left(A L_g\right)} + V_g\,\frac{1}{A^2}\left(-\frac{3}{W_b W_g + W_g^2}\right)\left(\frac{1}{\cosh\left(A L_g/2\right)} - 1\right) \quad (20)$$

Now we are going to investigate the variation of potential with device parameters and applied voltages. In this work, the analysis has been carried out for the GNR-FET with the following parameters fixed as: ε=3.9(for SiO_2), d=60 nm, v=10^6 m/s, T=800 K, W_b=100 nm, W_g=30 nm. The other parameters L_g, V_g, V_b and V_d were varied to see the effect of change of these parameters on electrical characteristics of the device.

Fig. 3 shows an example of the spatial distribution (along the channel, i.e., in the x direction) of the electric potential in the active region (under the top gate) calculated for a GNR-FET with L_g = 300 nm, V_b = 2.0 V, V_d = 0.5 V and different values of V_g. We see that the absolute value of potential increases with the increase of absolute value of the top gate voltage V_g. That is, the barrier for electrons increases with increasing $|V_g|$.

Published By:
Blue Eyes Intelligence Engineering
& Sciences Publication Pvt. Ltd.

Again, the spatial variation of potential at different drain voltages has been calculated with L_g = 300 nm, V_g = - 0.3 V, V_b = 2.0 V and presented in Fig. 4. It shows that at the source side (at x = - L_g/2), potential level doesn't change with drain voltage, i.e., the barrier for the electrons propagating from the source is insensitive to the drain voltage. On the other hand, at the drain side (at x = + L_g/2), potential level increases with increasing V_d, i.e., the barrier for the electrons propagating from the drain is increasing with increasing V_d.

The effect of gate length (L_g) on the potential in the channel has been investigated. The spatial distribution of potential in the channel for different gate lengths is shown in Fig. 5. The potential increases with the decrease of gate length at both source and drain sides; however, the change at the drain side is more. That is, the barrier for the electrons is increasing at both source and drain sides with decreasing L_g, however the effect at the drain side is stronger than source side.

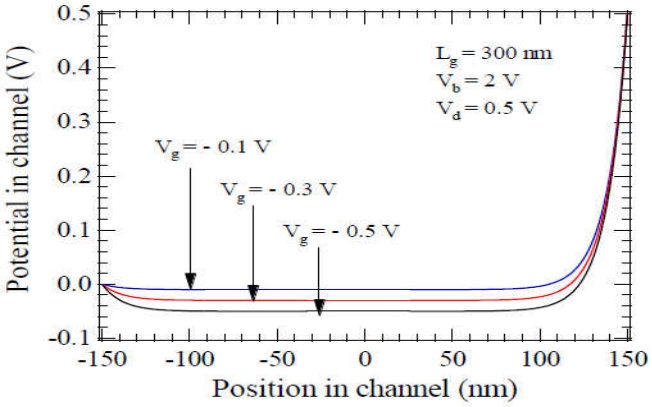

Fig. 3 Spatial distribution of potential in GNR-FET at different gate voltages.

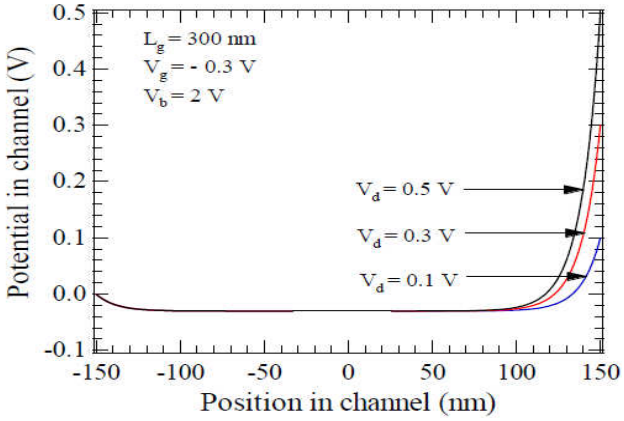

Fig. 4 Spatial distribution of potential in GNR-FET at different drain voltages.

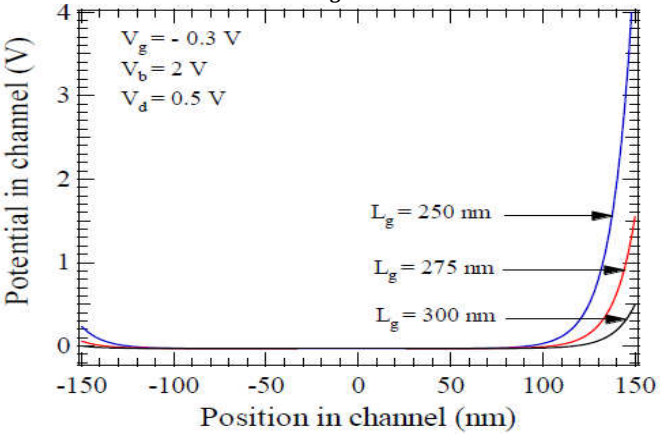

Fig. 5 Spatial distribution of potential in GNR-FET for different gate lengths.

IV. Current-Voltage Characteristics of Low Bandgap GNR-FET

The following formula for the drain current density can be derived considering that the current is caused by the electrons overcoming the potential barrier under the top gate [4].

$$J = \frac{2e}{\pi\hbar d}\left(\int_{p_m^s}^{\infty} dp v_p f_p^s - \int_{p_m^d}^{\infty} dp v_p f_p^d\right) \quad (21)$$

Here, v_p is the velocity of the electron with momentum p in the lowest sub-band of the nanoribbon conduction band and p_m^s and p_m^d are the momenta of the electrons with energies $e|\varphi_m|$ and $e(|\varphi_m|+V_d)$ respectively. Considering the electron and hole gases are non-degenerate, the electron and hole distribution functions in the sub-bands with n = 1 is stated below [4].

$$f_p^{\mp} = \exp\left(\frac{\pm e\varphi \pm E_F - \sqrt{v^2p^2 + \Delta^2/4}}{K_BT}\right)$$

Also, the value of v_p is,

$$v_p = v^2 \frac{p}{\sqrt{v^2p^2 + \Delta^2/4}}$$

Integration of (21) gives the following equation of drain current density.

$$J = \alpha \exp(\beta e\varphi_m)\left[\exp\left(\sinh^{-1}(\beta\gamma V_b)\right)\exp\left(-\beta\sqrt{\frac{\Delta^2}{4} + (e|\varphi_m|)^2}\right)\right.$$
$$\left. - \exp\left(\sinh^{-1}(\beta\gamma(V_b - V_d))\right)\exp\left(-\beta\sqrt{\frac{\Delta^2}{4} + (e(|\varphi_m| + V_d))^2}\right)\right] \quad (22)$$

Here,

$$\alpha = \frac{2eK_BT}{\pi\hbar d};\ \beta = \frac{1}{K_BT};\ \gamma = \frac{e\hbar dv}{32eW_b}$$

Equation (22) shows the dependence of drain current density on different parameters of the device and applied voltages. Here φ_m is given by (20).

Now let us look at the behaviour of drain current variation with different applied voltages. To see the effect of top gate voltage on the drain current of a low band gap GNR-FET, drain current has been calculated as the function of drain voltage for different top gate voltages with certain values of back gate voltage and gate length. Fig. 6 presents the results calculated for different top gate voltages with back gate voltage of 2 V and gate length of 300 nm. We see that drain current increases with drain voltage but current becomes insensitive to drain voltage after reaching saturation. That is, the device exhibits the standard FET characteristics. If the magnitude of top gate voltage is increased the drain current level is reduced; this is because the barrier for electrons increases with increasing top gate voltage, mentioned earlier.

Similarly, the effect of back gate voltage has been estimated by calculating drain current as the function of drain voltage for different back gate voltage with certain values of top gate voltage and gate length. Fig. 7 shows the drain current of a low band gap GNR-FET as a function of the drain voltage for different back gate voltages with top gate voltage of -1 V and gate length of 300 nm. We see that if the back gate voltage is increased the drain current level is increased. That is, the effects of top gate voltage and back gate voltage on the drain current are opposite, however, drain current is

Published By:
Blue Eyes Intelligence Engineering
& Sciences Publication Pvt. Ltd.

controllable by gate voltage and hence applicable in digital and analog circuits.

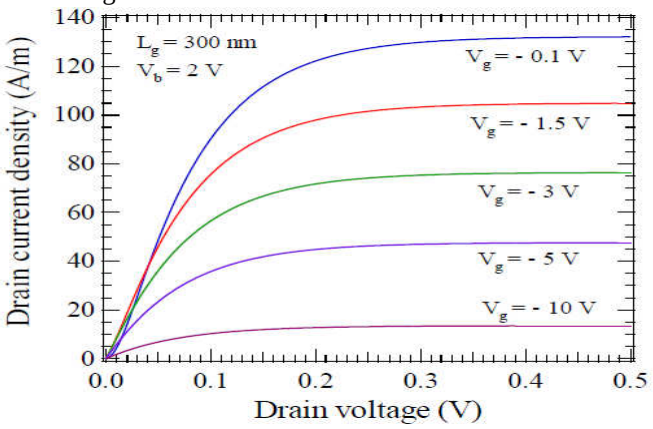

Fig. 6 Drain current density versus drain voltage of a low bandgap GNR-FET at different top gate voltages, with back gate voltage of 2 V and gate length of 300 nm.

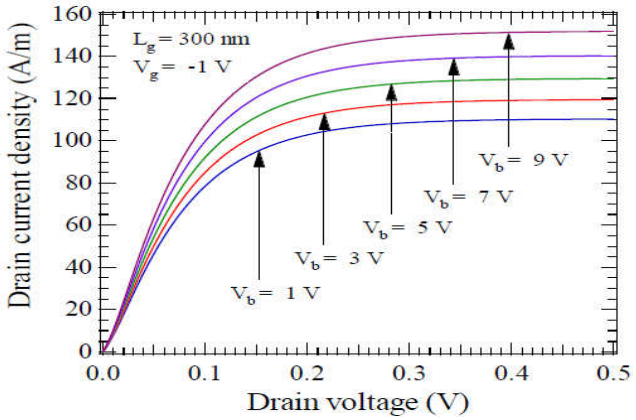

Fig. 7 Drain current density versus drain voltage of a low bandgap GNR-FET at different back gate voltages, with top gate voltage of -1 V and gate length of 300 nm.

To see the sensitivity of drain current to the top gate voltage, saturated drain currents of GNR-FET were calculated for different top gate voltages with gate length of 300 nm, back gate voltage of 2V, and drain voltage of 0.5V; the results are plotted in Fig. 8.

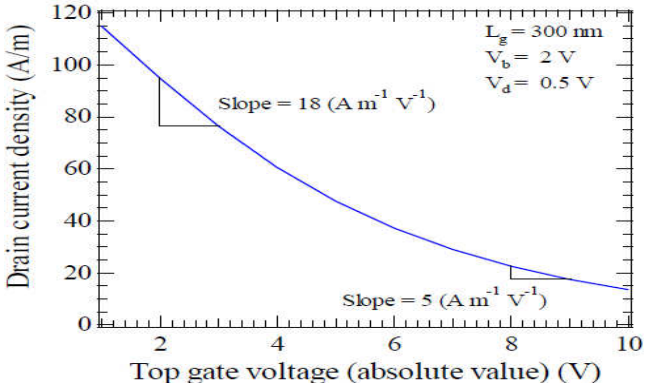

Fig. 8 Saturated drain current versus top gate voltage of a low bandgap GNR-FET, with gate length of 300 nm, back gate voltage of 2 V and drain voltage of 0.5 V.

We found that drain current changes with top gate voltage at the rate of minimum 5 $Am^{-1}V^{-1}$ and maximum 18 $Am^{-1}V^{-1}$.

Similarly, to see the sensitivity of drain current to back gate voltage, saturated drain currents were calculated for different back gate voltages with gate length of 300 nm, top gate voltage of -2V, and drain voltage of 0.5 V and plotted in Fig. 9. We observed that drain current changes with back gate voltage at a constant rate 4.5 $Am^{-1}V^{-1}$, which is less than the minimum rate of change of drain current caused by top gate voltage. That is, drain current is highly sensitive to top gate voltage compared to back gate voltage.

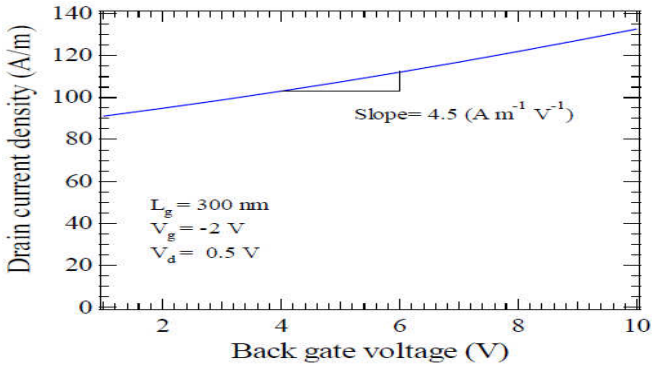

Fig. 9 Saturated drain current versus back gate voltage of a low bandgap GNR-FET, with gate length of 300 nm, top gate voltage of -2 V and drain voltage of 0.5 V.

The analytical expressions and results of potential and drain current of low bandgap GNR-FET, presented in this paper, are similar to those presented by Ryzhii *et al.* [4], however, there is a little difference, this logical because they worked with high bandgap FET whereas our work is with low bandgap FET; the results of our work are in good agreement with the published works in this area.

V. Conclusion

The analytical modeling of electric potential in the channel of low bandgap GNR-FET shows that potential increases with the increase of absolute value of top gate voltage, i.e., barrier for electrons increases with top gate voltage. The effect of drain voltage shows that potential is insensitive to drain voltage at the source side but potential increases with drain voltage at the drain side. The study of the effect of gate length reveals that potential increases at both source and drain sides with the decrease of gate length but the effect at the drain side is dominant. The analytical modeling of drain current of low bandgap GNR-FET shows that drain current versus drain voltage exhibits standard FET characteristics. Drain current level decreases with the increase of top gate voltage level, whereas, drain current level increases with the increase of back gate voltage, that is, the effects of top gate voltage and back gate voltage on drain current are opposite, however, drain current is controllable with gate voltage. Drain current is found highly sensitive to top gate voltage compared to back gate voltage. This work would be helpful to analyze low bandgap GNR-FET and to optimize the device parameters and applied voltages to have better performance.

Acknowledgment

The authors would like to acknowledge with thanks the supports from King Abdulaziz University, Saudi Arabia; Iowa State University, USA; and University of Toronto, Canada to complete the work.

References

1. Shazia Hassan, Humaira, and Mamoona Asghar, “Limitation of silicon based computation and future prospects,” in *Proc. ICCSN’10*, 2010.
2. A. K. Geim and K. S. Novoselov, “The rise of graphene,” Nat. Mater., vol. 6, 2007, p. 183.

Published By:
Blue Eyes Intelligence Engineering
& Sciences Publication Pvt. Ltd.

3. Niraj K. Jha and Deming Chen, Nanoelectronic Circuit Design, Springer, 2011, pp. 349–376.
4. V. Ryzhii, M. Ryzhii, A. Satou, and T.Otsuji, “Current-voltage characteristics of a graphene-nanoribbon field-effect transistor,” J. Appl. Phys., vol. 103, 2008, p. 094510.
5. V. V. Cheianov and V. I. Fal'ko, "Selective transmission of Dirac electrons and bassistic magnetoresistance of n-p junctions in graphene," Phys. Rev. B, vol. 74, 2006, p. 041403.
6. A. Ossipov, M. Titov, and C. W. J. Beenakker, "Reentrance effect in a graphene n-p-n junction coupled to a superconductor," Phys. Rev. B, vol. 75, 2007, p. 241401.
7. Victor Ryzhii, Maxim Ryzhii, and Taiichi Otsuji, “Tunneling current-voltage characteristics of graphene field-effect transistor,” Applied Physics Express, vol. 1, 2008, p. 013001.
8. Melinda Y. Han, Barbaros Ozyilmaz, Yuanbo Zhang, and Philip Kim, “Energy Band Gap Engineering of Graphene Nanoribbons,” PRL 98, 2007, p. 206805.
9. A. A. Sukhanov and Yu. Ya. Tkach, “Equation for the surface potential distribution in two-dimensional layer systems,” Sov. Phys. Semicond., vol. 18, 1984, p. 797.
10. V. I. Ryzhii and I. I. Khmyrova, "Current crowding effect in hot-electron heterostructure transistors," Sov. Phys. Semicond., vol. 22, 1988, p. 807.

Md. Shofiqul Islam received BSc and MSc degree both in Electrical and Electronic Engineering from Bangladesh University of Engineering and Technology, Dhaka, Bangladesh, in 1999 and 2002, respectively. He obtained his PhD degree in Electronic and Information Engineering from Toyohashi University of Technology, Toyohashi, Japan in 2007. He is currently working as an Associate Professor in the Department of Electrical and Computer Engineering in King Abdulaziz University, Saudi Arabia. He has long experience to work with the fabrication of Si microneedles and electronic devices within the microneedles for biomedical applications. His current research interests include MEMS, electronic devices, sensors, solar cells (carbon & organic).

Tanvir Muntasir obtained BSc degree in Electrical and Electronic Engineering from Bangladesh University of Engineering and Technology, Dhaka, Bangladesh, in 2011. He is currently pursuing his PhD study in Electrical Engineering in Iowa State University, USA. His research interests include electronic devices, defect metrology in semiconductor thin films.

Shuvomoy Das Gupta received BSc degree in Electrical and Electronic Engineering from Bangladesh University of Engineering and Technology, Dhaka, Bangladesh, in 2011. Now he is working for PhD degree in University of Toronto, Canada. His research interests include mathematical optimization, game theory, constraint programming.

Published By:
Blue Eyes Intelligence Engineering
& Sciences Publication Pvt. Ltd.